Finite-temperature properties of ultra-thin lead films on gold (110) surfaces

1997 J. Phys.: Condens. Matter 9 5719

(http://iopscience.iop.org/0953-8984/9/27/005)

J. Phys.: Condens. Matter **9** (1997) 5719–5735. Printed in the UK PII: S0953-8984(97)80855-7

Finite-temperature properties of ultra-thin lead films on gold (110) surfaces

K De'Bell and D Imeson

Physics Department, Trent University, Peterborough, Canada K9J 7B8

Received 10 January 1997

Abstract. At low coverages, lead adatoms form a single layer on the gold (110) surface. However, if a critical coverage θ_c is exceeded, a second adlayer forms. At zero temperature, various properties such as the energy and atomic spacing of atoms in the first adlayer are discontinuous at θ_c. The effects of temperature on the discontinuities and location of θ_c are reported. Results for clean Au(110) and Pb(110) surfaces are also reported.

1. Introduction

The structural properties of thin metal-on-metal films may be investigated by a variety of experimental techniques [1, 2]. Determinations of these structures by computer simulation have two important roles. First, comparisons of simulations with existing experimental results provide a test of our understanding of atomic interactions and the reliability of simulation results based on theoretical models. Second, once a combination of theoretical model and simulation technique has been shown to be reliable for a given group of metals, simulations may be used to predict suitable combinations of adsorbate and substrate for specific applications, thus reducing the time and expense required for final experimental determinations of the required combinations.

In experimental studies of lead (Pb) on the gold (Au) (110) surface, it is observed that a variety of structures occur depending on the coverage [2]. The lead forms a single simple adlayer until a saturation coverage of $\theta = 6/7 \approx 0.86$ is reached. (The value of the saturation coverage was determined from LEED patterns.) If the saturation coverage is exceeded, a second adlayer begins to form, and at higher coverages, a variety of surface alloys are observed.

Recently, simulation studies based on an embedded-atom method (EAM) model for Pb on Au(110) were reported [3]. Although limited to zero temperature, the results of these studies were consistent with the experimental studies in that a saturation coverage $\theta_c < 1$ was observed. The simulations also demonstrated that discontinuities occur in such properties as the energy and atomic spacing of the atoms in the first adlayer at the saturation coverage. However, the zero-temperature value of the saturation coverage obtained in the simulations, $\theta_c = 0.91 \pm 0.01$, was slightly but significantly higher than the saturation coverage determined in the experiments, and it was speculated that the difference was due to finite-temperature effects.

Here simulation studies of Pb on Au(110) at finite temperatures are reported. Both the effect of temperature on the value of the saturation coverage and the effect of temperature on the discontinuities are reported. In section 2 the EAM model is briefly described and test

0953-8984/97/275719+17$19.50

results for clean Pb and Au surfaces are compared with experiment and other theoretical studies. Results for Pb on Au(110) up to a coverage of $\theta = 1.1$ are given in section 3. The study is summarized and the reliability of the method discussed in section 4.

2. Parameter fitting for the EAM

In this study the equations of motion were solved by a molecular dynamics program based on the velocity form of the Verlet algorithm. The atomic interactions were calculated using the EAM. The energy of atom i due to the surrounding atoms is assumed to consist of two parts, a two-body interaction ϕ and an embedding term $F(\rho_i)$ which depends on the local electron density ρ_i:

$$E_i = F(\rho_i) + \frac{1}{2}\sum_{j\ (\neq i)} \phi(r_{ij}). \tag{1}$$

The embedding function and two-body interaction are expressed in terms of a number of adjustable parameters which can be fitted to bulk properties of the solid. According to the prescription of Mei *et al* [4] these take the following forms:

$$F(\rho) = -E_c\left[1 - \frac{\alpha}{\beta}\ln\left(\frac{\rho}{\rho_e}\right)\right]\left[\frac{\rho}{\rho_e}\right]^{\alpha/\beta} - \frac{1}{2}\sum_m s_m\phi\left(p_m r_{1e}\left[1 - \frac{1}{\beta}\ln\left(\frac{\rho}{\rho_e}\right)\right]\right) \tag{2}$$

$$\phi(r) = \phi_e\left[1 + \delta\left(\frac{r}{r_{1e}} - 1\right)\right]\exp\left[-\gamma\left(\frac{r}{r_{1e}} - 1\right)\right]. \tag{3}$$

E_c, r_{1e}, and ϕ_e are the cohesive energy, equilibrium nearest-neighbour distance, and value of the two-body interaction at the equilibrium nearest-neighbour distance respectively. s_m and p_m are the number of atoms in the mth shell of atoms surrounding atom i, and the equilibrium value of the ratio of the distance between atom i and an atom in the mth shell and the nearest-neighbour distance respectively. In the studies reported here, contributions to the energy of the ith atom are calculated only from neighbouring atoms within a sphere of radius $1.6r_{1e}$ centred on atom i. This distance lies between the second and third shell of atomic neighbours in the equilibrium system.

The embedding function, F, is expressed as a function of the local electron density ρ, which may be calculated from the known locations of neighbouring atoms and the assumed functional form for the variation of electronic density with distance [4]:

$$\rho(r) = \rho_e\exp\left[-\beta\left(\frac{r}{r_e} - 1\right)\right]. \tag{4}$$

(In practice, this exponential form was approximated by a fifth-order polynomial in the simulation program as described by Mei *et al* [4].) Early papers using the EAM determined the parameters in the functional form for the electron density by matching the functional form to data from Hartree–Fock calculations. However, Johnson noted that this method for determining β in equation (4) is not robust, and developed an alternative method in which β is treated as an adjustable parameter [5]. Following this procedure, there are six adjustable parameters in the model: $\alpha, \beta, \gamma, \delta, \rho_e$, and ϕ_e. These are determined by matching the properties of the model to six experimentally determined quantities: the atomic volume Ω, the bulk modulus B, the shear modulus G, the cohesive energy E_c, the unrelaxed vacancy energy E_{UF}, and the elastic constant C_{12}. In summary, the parameters α, ρ_e, and β are determined immediately by fitting the properties of the model to match the experimental

Table 1. Experimental values used in the parametrization of the EAM functions, and the resulting parameter values for gold and lead. The experimental input parameters are the same as those used by Mei *et al* [4] and Karimi *et al* [15] in previous EAM studies of gold and lead respectively. However, the EAM parameters differ from those in the earlier studies because of differences in the fitting procedures.

	Au	Pb
Input experimental values		
G (eV Å^{-3})	0.1935	0.0853
C_{12} (eV Å^{-3})	0.9799	0.2834
E_c (eV)	3.93	2.09
B (eV Å^{-1})	1.042	0.3046
Ω (Å^3)	16.98	30.32
r_1 (Å)	2.88	3.50
Atomic mass (kg)	3.27×10^{-22}	3.44×10^{-22}
Calculated parameters		
ρ_e	0.2314	0.0689
α	6.37	6.31
β	7.127	8.200
γ	7.747	9.708
δ	3.945	0.000
ϕ_e	0.297	0.415
C_{12} (eV Å^{-3}) (calculated)	0.9799	0.2783

values of Ω, E_c, and B [5], and the remaining parameters are determined by noting that E_{UF}, G, and C_{12} may be expressed in the following forms [6]:

$$E_{UF} = K_E + \phi_e[f_E(\gamma) + \delta g_E(\gamma)] \tag{5}$$

$$G = \phi_e[f_G(\gamma) + \delta g_G(\gamma)] \tag{6}$$

and

$$C_{12} = K_C + \phi_e[f_C(\gamma) + \delta g_C(\gamma)]. \tag{7}$$

In these equations, the Ks are constants and the fs and gs are functions of only one unknown, γ. Equation (5) and equation (6) may then be rewritten as expressions for ϕ_e and δ in terms of the experimental values of E_{UF} and G, and γ. Substituting these into equation (7), an expression for C_{12} in terms of only one unknown parameter, γ, is obtained. γ may then be varied to minimize the absolute difference between the calculated and experimental values for C_{12}. Once γ is determined, ϕ_e and δ may be calculated. This method has the advantage that all of the physical properties except C_{12} used in the fitting procedure are fitted exactly, and it is not necessary to resort to the approximate form for E_{UF} used by Johnson in the fitting procedure [6]. Values of the parameters obtained for lead and gold in this way are shown in table 1.

The EAM model parameters for each metal are determined from the bulk properties of that metal only. When the model is used to model the interactions of two or more species of atoms, the two-body potential for interactions between dissimilar atoms must be constructed. Following Johnson [5], the two-body potential for dissimilar atoms was taken to be

$$\phi^{ab}(r) = \frac{1}{2}\left[\frac{f^b(r)}{f^a(r)}\phi^{aa}(r) + \frac{f^a(r)}{f^b(r)}\phi^{bb}(r)\right]. \tag{8}$$

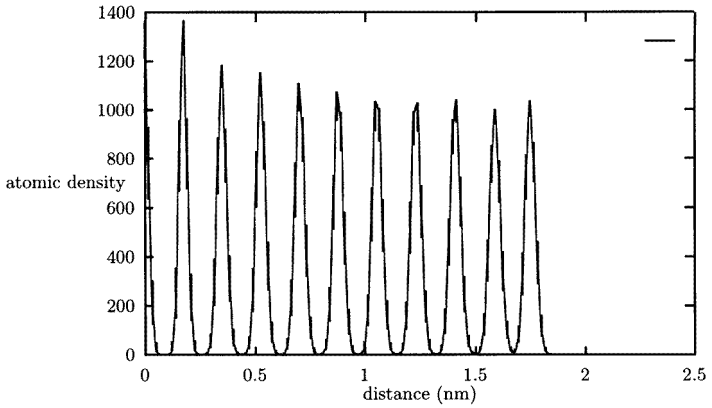

(a)

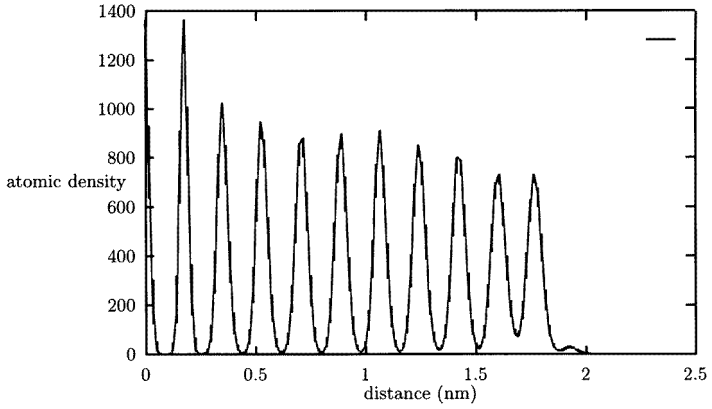

(b)

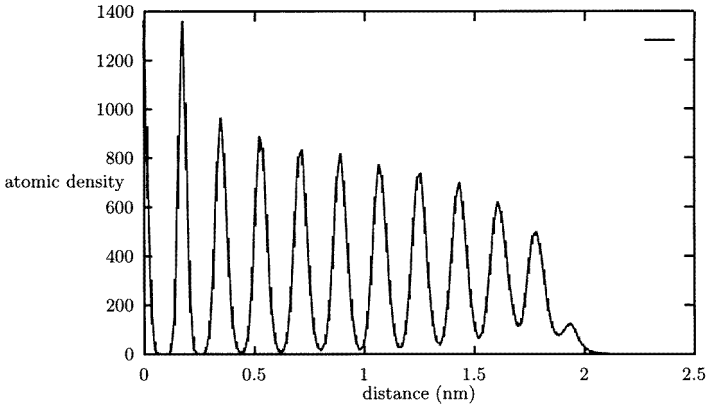

(c)

Figure 1. The atomic density profile as a function of the distance from the bottom fixed layer in a simulation of Pb, at $T = 200$ K (a), 450 K (b), 550 K (c), 600 K (d), 650 K (e), and 700 K (f).

$f_a(r)$ and $f_b(r)$ are the single-atom electron densities at distance r from an atom of type a or b respectively in the pure metal. As the EAM parameters are determined solely by the

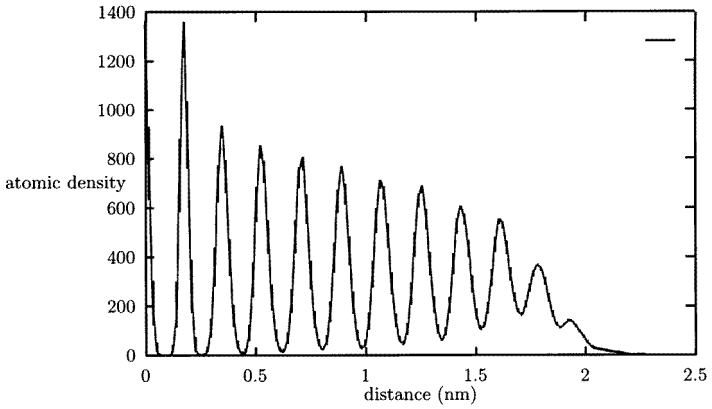

(d)

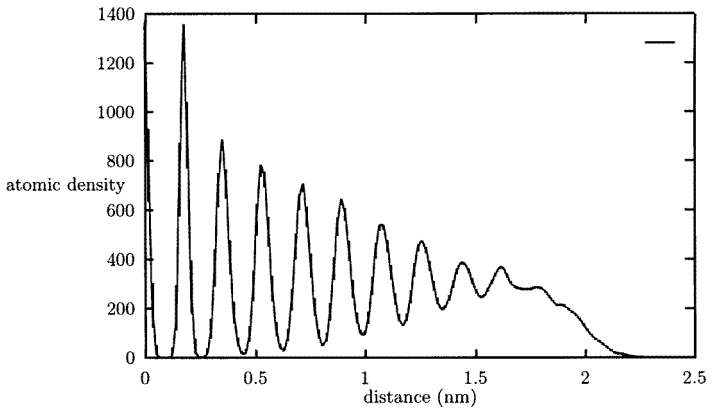

(e)

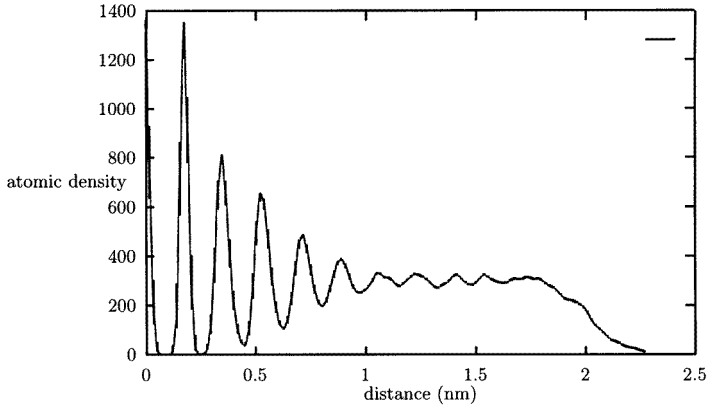

(f)

Figure 1. (Continued)

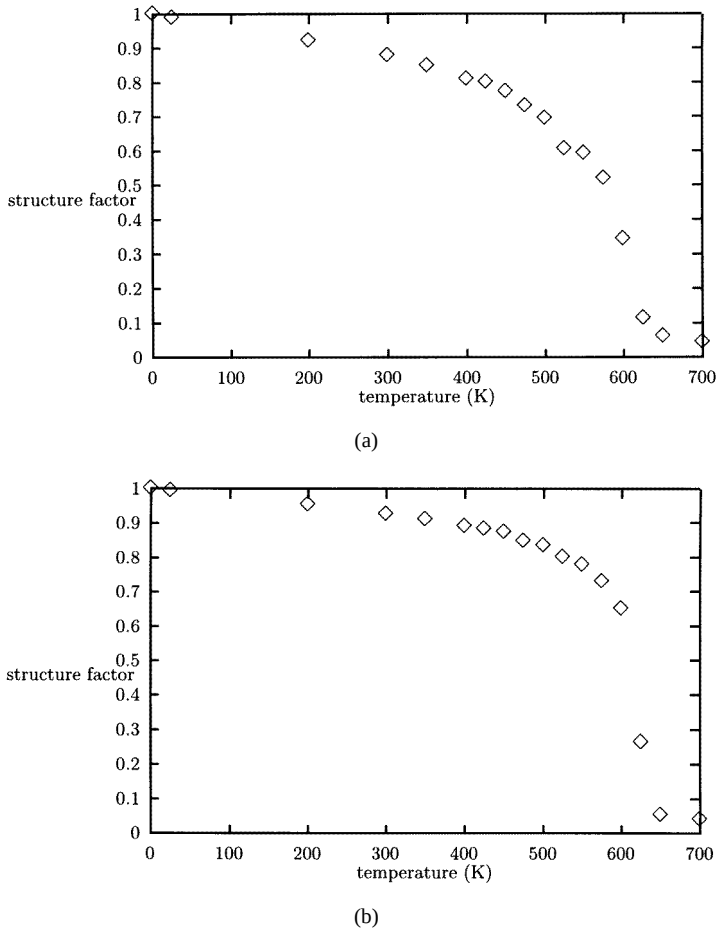

Figure 2. The structure factor for the lead (110) surface evaluated at one reciprocal-lattice vector, as a function of temperature. Top-layer $(1\bar{1}0)$ direction (a), second-layer $(1\bar{1}0)$ direction (b), top-layer (001) direction (c), and second-layer (001) direction (d).

bulk properties of the metals, it is highly desirable to determine the reliability of the models for determining surface properties. Consequently, the EAM/MD was used to determine the surface melting temperature of both the pure Pb(110) surface and the pure Au(110) surface. Two types of configuration were considered. In the first, the metal is a slab with two free surfaces and periodic boundary conditions applied in directions parallel to the surfaces. In the second, the top layer of the simulated sample is a free surface and the sample is truncated at its lower surface by two layers of atoms fixed in their bulk equilibrium positions. The fixed layers in this second type of configuration are intended to mimic the effects of the bulk of the sample in thick substrates. In the case of the first type of configuration, the samples were eleven layers thick. In the case of the second type of configuration, samples of both eleven layers and of twenty layers were used. Estimates of zero-temperature quantities such as the surface energy showed little dependence on the configuration chosen [6] and, therefore, the 11-layer sample with two fixed 'bulk' layers was used for most of the finite-temperature simulations.

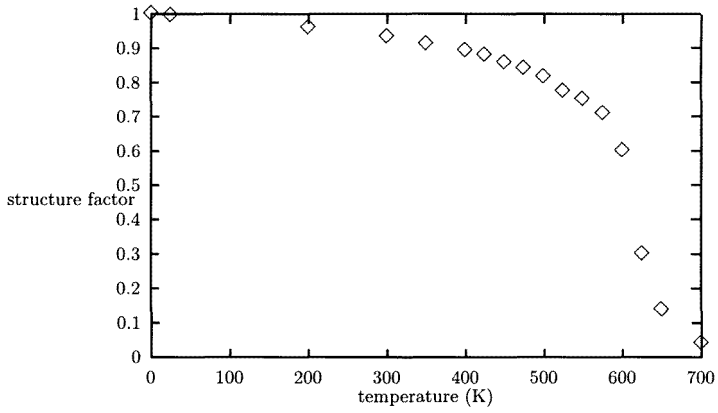

(c)

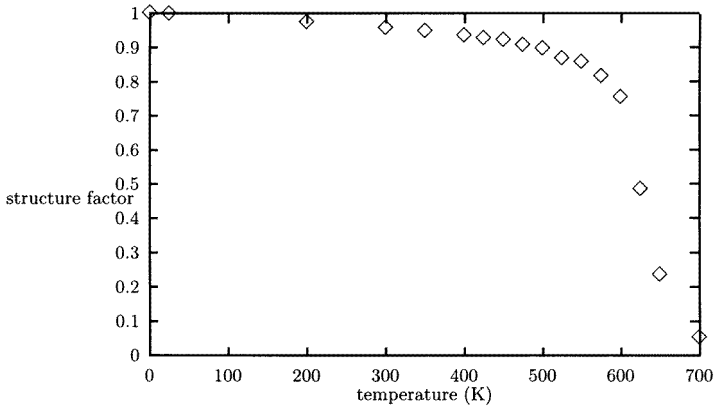

(d)

Figure 2. (Continued)

3. Transitions on clean Au(110) and Pb(110) surfaces

In a typical run of the simulation program, the temperature was increased from zero at a rate of 5 K ps^{-1} until a temperature equal to approximately half the expected melting temperature was reached. The temperature increase was then continued at a rate of 1 K ps^{-1}. When data were to be collected at a given temperature, the system was maintained at this temperature for 35 ps before data collection started. Data were then collected over a 40 ps period. As the temperature of the system was raised from zero to approximately 1000 K, it was necessary to allow for thermal expansion of the fixed bulk layers. This was done by calculating the thermal expansion using experimentally determined values for the coefficient of thermal expansion, and adjusting the dimensions of the sample accordingly. For gold the coefficient of thermal expansion used was 1.4×10^{-5} m K^{-1} and for lead 2.9×10^{-5} m K^{-1} was used [7].

Prior to the surface melting of lead (110), a roughening transition is expected [8]. At this transition, atoms initially in the top layer of the sample move up into interstitial sites on top of the layer. The atomic density profiles calculated at various temperatures in the simulation are shown in figure 1. (For the purpose of calculating the atomic density profile,

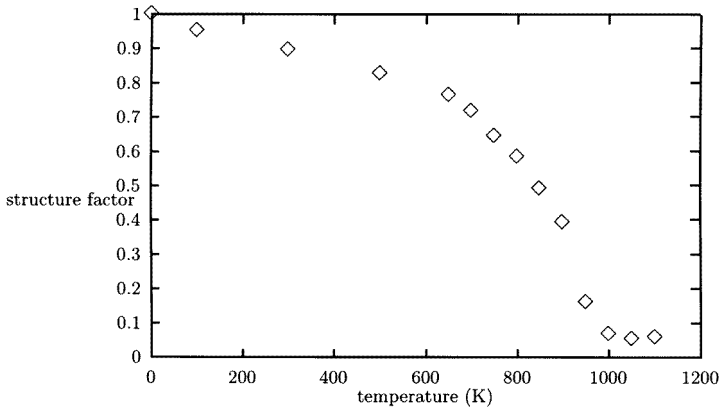

(a)

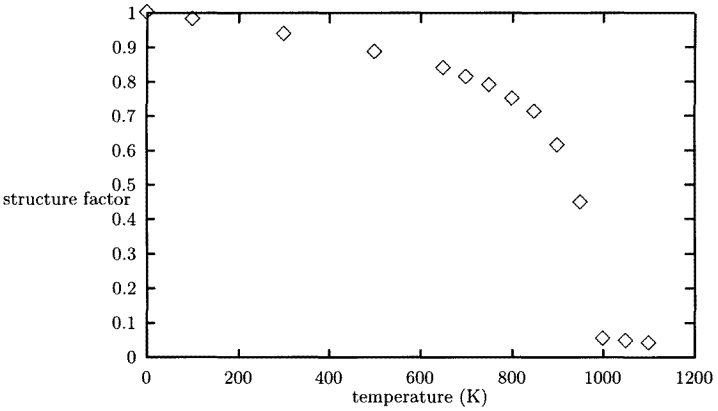

(b)

Figure 3. The structure factor for the gold (110) reconstructed surface evaluated at one reciprocal-lattice vector parallel to the missing-row (the $(1\bar{1}0)$ direction) top layer (a) and second layer (b), and evaluated at one reciprocal-lattice vector perpendicular to the missing-row (the (001) direction) top layer (c) and second layer (d).

each atom was represented by a Gaussian distribution with a width of approximately a tenth of the interlayer spacing.) The roughening transition can be identified by noting that a small peak corresponding to atoms on top of the original surface layer has appeared in the density distribution by the time the temperature reaches 450 K. This peak is absent at 400 K. Consequently the roughening transition occurs in the range $T_R = 425 \pm 25$ K. This is in excellent agreement with experimental values for the roughening transition temperature which lie in the range 390 to 450 K [8]. It is also in excellent agreement with a previous simulation study result of $T_R = 400$ K [9].

The melting of the surface can also be observed in the atomic density profile. As can be seen in figure 1, the peak in the atomic density corresponding to the original surface layer is still distinct at 600 K but is no longer distinct at 650 K. A more precise estimate of the surface melting transition temperature was obtained by considering the structure factor,

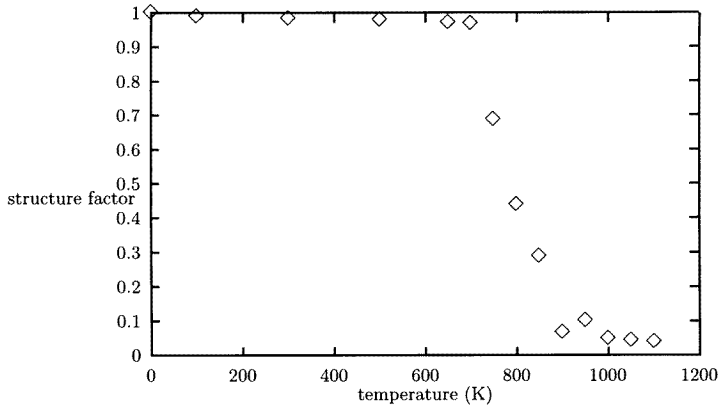

(c)

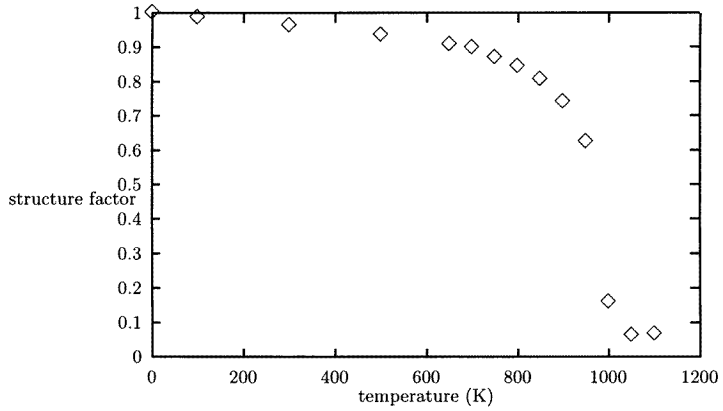

(d)

Figure 3. (Continued)

S, defined by

$$S(\boldsymbol{g})^2 = \left\langle \frac{1}{n^2} \left| \sum_{i \in l} \exp(-\boldsymbol{g} \cdot \boldsymbol{r}_i) \right|^2 \right\rangle. \tag{9}$$

This structure factor can be constructed for each layer l in the sample. The sum is over all atoms in the chosen layer, and n is the number of atoms in the layer. Figure 2 shows the structure factor evaluated at a reciprocal-lattice vector for the top two layers in the sample as a function of temperature. The surface melting temperature was determined from the inflection point of the structure factor curve for the top layer, resulting in an estimate of $T_M = 625 \pm 25$ K which is consistent with the range determined from the atomic density profile. This value is above the range of 520 to 580 K which experimental results would indicate [8].

The clean gold (110) surface has a reconstructed 1×2 (missing-row) structure [10]. All of the simulations of pure gold were started with the top layer in the 1×2 configuration. Consequently, two transitions were anticipated. At the first transition the 1×2 structure is lost; however, the top-layer atoms remain essentially in the interstitial positions. At the second transition the surface layer melts fully. In figure 3 the structure factor at

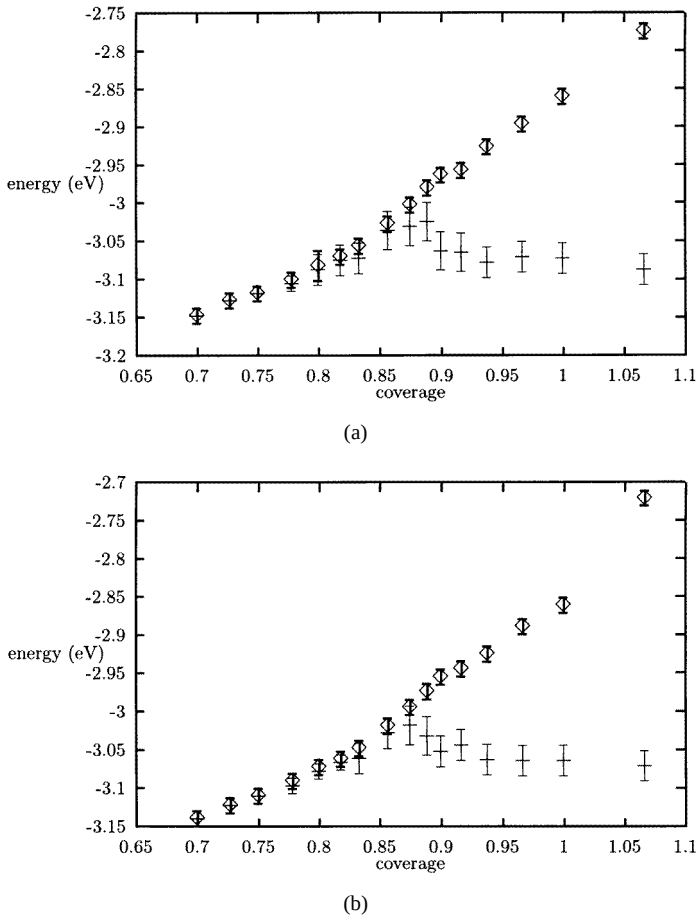

Figure 4. The average energy of all of the lead atoms (upper line) and the average energy of lead atoms in the first adlayer (lower line), at $T = 50$ K (a), 100 K (b), 200 K (c), and 300 K (d).

reciprocal-lattice vectors parallel to the missing rows and perpendicular to the missing rows are shown. We denote these directions as the x- and y-directions respectively. The structure factor for the y-direction drops steeply just above 800 K, indicating the loss of the 1×2 structure. However, the structure factor for the x-direction does not drop to a value close to zero until a temperature of almost 1000 K is reached. On the basis of these curves, the disordering temperature for the 1×2 phase is estimated to be 860 ± 40 K and the surface melting temperature is estimated to be 980 ± 40 K. The value for the disordering transition temperature is higher than reported experimental values, which fall in the range 693 to 725 K [10, 11]. While the value is very close to the value of 850 K found in a previous simulation [12], another EAM study obtained a value of 570 K [13]. However, this later study used only nearest-neighbour interactions. The melting transition temperature is also in good agreement with that found in a simulation study by Ercolessi *et al* [12], but is significantly higher than the experimental value of 770 K [14].

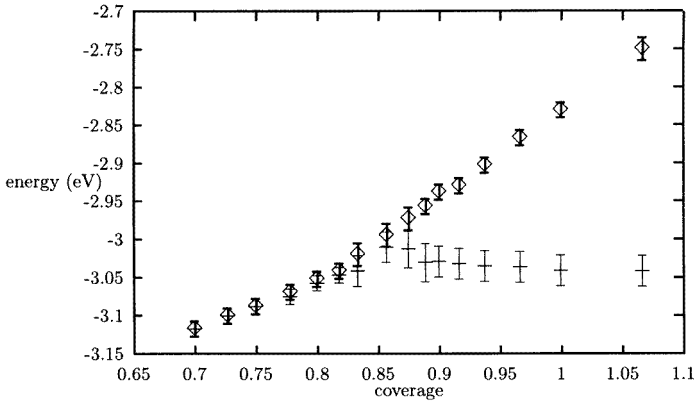

(c)

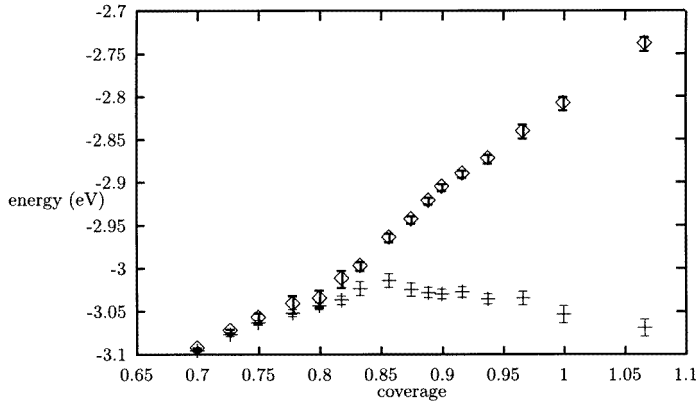

(d)

Figure 4. (Continued)

4. Pb on Au(110)

Using the EAM parameters determined for pure gold and pure lead, the properties of thin lead films on the Au(110) surface have been simulated. The system consisted of nine Au layers with the bottom two fixed in bulk Au positions. Lead atoms were placed on the free surface of the gold substrate for various coverages, and the sample was maintained at the chosen temperature. The coverage used here is the number of lead atoms divided by the number of gold atoms in a perfect gold surface layer. At each coverage several simulations were performed, each starting from a different configuration of lead atoms.

Following the zero-temperature study performed previously [3], the total energy of the lead atoms and the energy of lead atoms in the first adlayer were calculated. The average spacing measured along the troughs of the Au(110) surface of Pb atoms in the first adlayer, and the average distance of the first adlayer from the gold surface were also calculated. In addition, the average thickness of the lead layer was calculated. For the purposes of this study, the thickness was defined to be

$$W = \sum_i x_i \Big/ \sum_i 1. \tag{10}$$

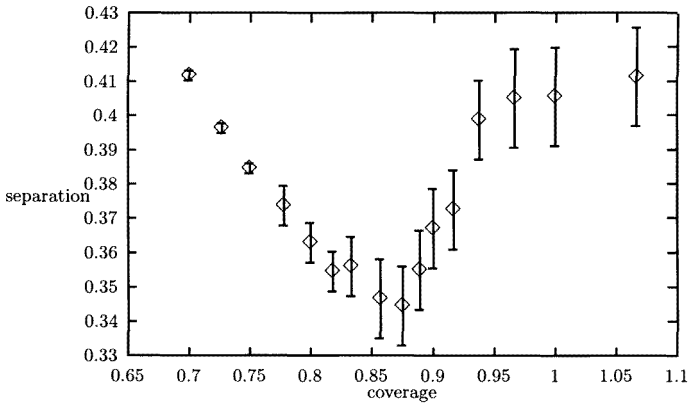

(a)

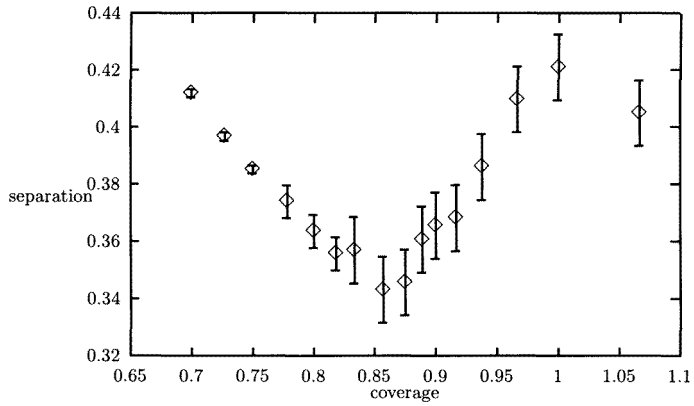

(b)

Figure 5. The nearest-neighbour separation of lead atoms along the troughs (namely, along $(1\bar{1}0)$) at $T = 50$ K (a), 100 K (b), 200 K (c), and 300 K (d).

The sum in this expression is over all lead atoms, and x_i is the distance of the ith lead atom from a plane placed between the gold surface and the first layer of lead atoms.

Figure 4 shows the average energy of all lead atoms, and the average energy of atoms in the first adlayer only for simulations performed at 50 K. In the previously reported zero-temperature study [3], the two curves coincide and the average energy increases with increasing coverage until the saturation coverage is reached. At the saturation coverage, there is a discontinuity in the average energy of the atoms in the first adlayer, and the energy of atoms in the first adlayer drops to a value below the value that was obtained just below the saturation coverage. Inspection of the configurations of lead atoms just below and just above the saturation coverage shows that lead atoms initially in the first adlayer move into the bridge sites and form the second adlayer at the saturation coverage. As a result of this, the separation of the atoms remaining in the first adlayer increases and the energy decreases. The curves obtained at finite temperature are qualitatively similar to those at zero temperature, except that the curves begin to separate at a much lower value of coverage ($\approx$0.75). Although the separation is less than the error bars, it is consistently present as the coverage is increased (see also comments in the summary). Both curves are

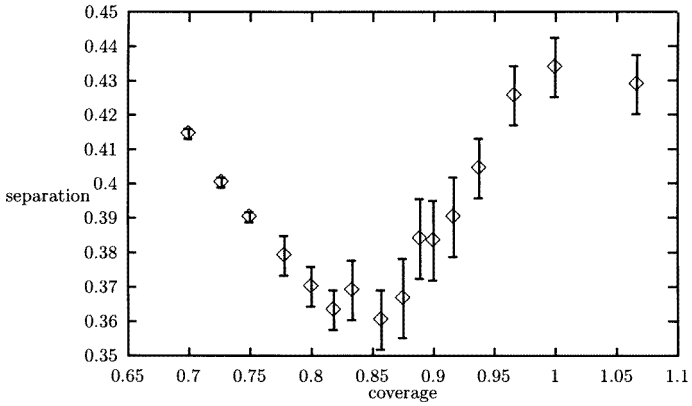

(c)

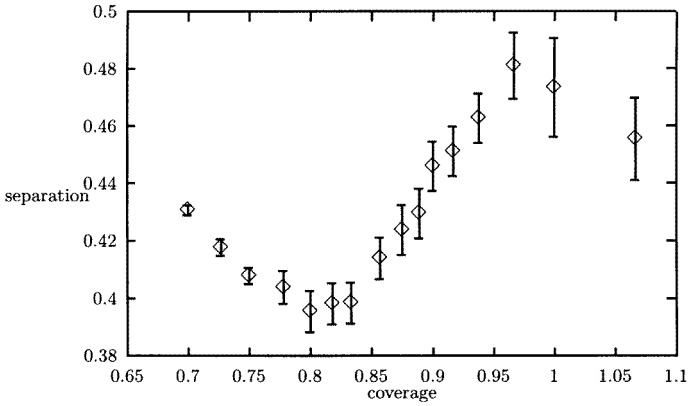

(d)

Figure 5. (Continued)

continuous and have positive slope, and the separation of the curves increases gradually as coverage increases further until a coverage of ≈ 0.9 is reached. In the vicinity of this value the average energy of atoms in the first adlayer drops rapidly, while the energy of atoms in the second layer continues to increase. This behaviour is essentially the same as is seen in the zero-temperature study, indicating that the same physical mechanisms of migration from the first adlayer into the second adlayer at a saturation coverage of ≈ 0.90 occur. The separation of the two curves at lower values of the coverage indicates that a fraction of the adatoms are thermally excited into second-layer positions even below the saturation coverage.

The behaviour of the nearest-neighbour distance measured along the (110) surface troughs for first-adlayer lead atoms is qualitatively similar to that found at zero temperature. There is an initial decrease in the separation with coverage which continues until the saturation coverage is reached. A rapid increase in the separation occurs at the saturation coverage. The principal change induced by the finite temperature is a smearing of the discontinuity (see figure 5). Similarly, the behaviour of the separation of the first adlayer and the gold surface at finite temperature is qualitatively similar to that found at zero temperature, but the smearing of the discontinuity increases with increasing temperature.

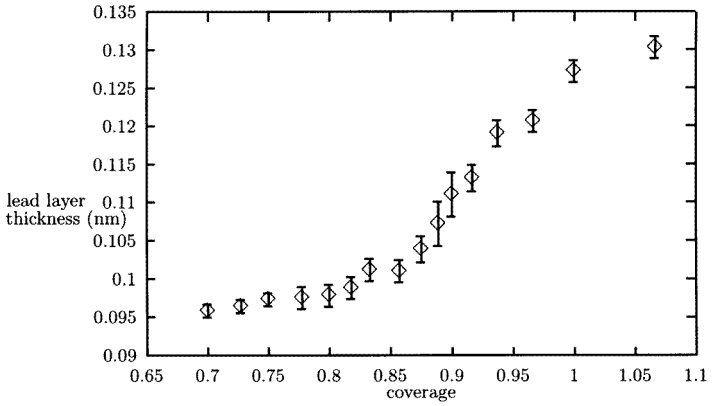

(a)

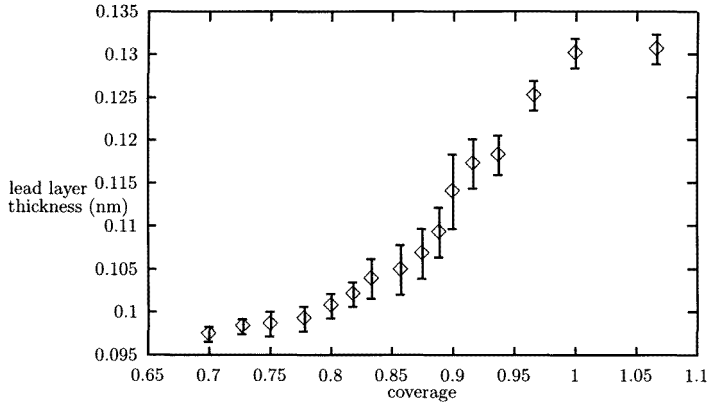

(b)

Figure 6. The variation of the lead layer thickness with coverage at $T = 50$ K (a) and 200 K (b). The layer thickness is determined according to equation (8).

The variation of the thickness of the lead layer with coverage is shown in figure 6. While the increase in the thickness is most rapid in the vicinity of the saturation coverage, the curve is relatively smooth, and it would be difficult to provide a precise estimate of the saturation coverage based on changes in the layer thickness alone for any of the finite temperatures studied.

In part, the extension of the Pb-on-Au(110) study to finite temperature was motivated by a need to determine whether the difference between the experimental value of the saturation coverage and the value obtained in the zero-temperature study was due to the temperature in the experimental system being finite. Inspection of the curves for the four functions discussed above shows that the rapid changes associated with the saturation coverage do move to slightly lower values of coverage as the temperature is increased. As the temperature is increased it becomes more difficult to assign a precise value for the saturation coverage, because of the increased smearing of the discontinuity. Here we take the saturation coverage to occur at the midpoint between the last point which shows a decrease in the nearest-neighbour separation (figure 5) with coverage and the next point. The values of saturation coverage obtained in this way are shown in figure 7. As shown in figure 7, the

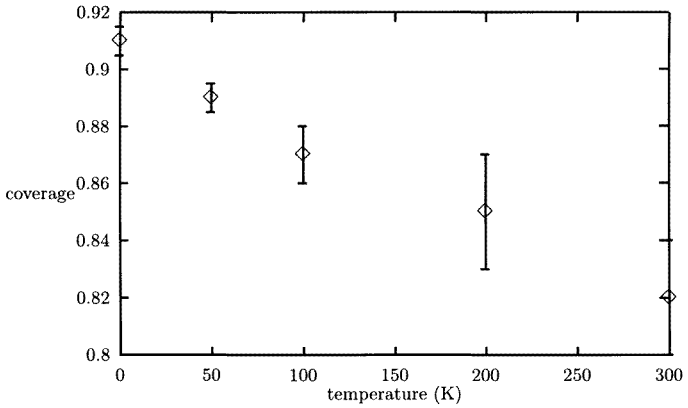

Figure 7. The variation of the saturation coverage with temperature. The saturation coverage is determined from the variation in the lead atom separation, as described in the text.

change from zero temperature to room temperature lowers the calculated θ_c as anticipated. The estimate of $\theta_c = 0.82 \pm 0.02$ at 300 K is slightly lower than the experimental value of $\theta_c \approx 0.86$. However, given the difficulty in determining the value of θ_c once the discontinuity in atomic separation has been significantly rounded by the finite-temperature effects, this discrepancy should probably not be considered significant.

5. Summary

In assessing the reliability of the EAM/MD method for determining the properties of ultra-thin metal films on gold substrates, the results of the study of lead on gold (110) reported above appear to be very promising. Not only does the method predict a saturation value for the coverage which is less than one lead atom/gold atom, but also the method is able to predict relatively small differences in the saturation value due to finite-temperature effects. Notice that the simulations also indicate that the precise coverage at which the second layer begins to form becomes increasingly difficult to determine with increasing temperature. Once these effects are taken into account, there is good quantitative agreement with experiment.

As the experimental work was based on LEED, the determination is in fact a determination of (ordered) structure in the Pb layer rather than a precise determination of the coverage. Consequently, a more direct comparison between experiment and simulation is provided by comparing the separation of the Pb atoms in the first layer just above the coverage at which the second layer starts. Using a value of 0.408 nm for the nearest-neighbour separation of gold atoms in the surface, the experimental determination of a 6/7 pattern implies that the Pb atoms are separated by approximately 0.476 nm along the troughs. In simulations with a temperature $T \leqslant 200$ K, the separation of the lead atoms at $\theta \approx 0.95$ is significantly less than the value implied by the experiments. However, if the temperature of the simulation is 300 K, the separation of the lead atoms (0.48 ± 0.02 nm) is very close to the experimental values. (It is perhaps also worth noting that the separation values of the Pb atoms even at coverages as low as $\theta \approx 0.7$ are significantly less than the interatomic spacing in bulk Pb. This may explain the initial separation of the energy curves at these relatively low coverages.)

Similarly, the method predicts a roughening transition for the pure lead (110) surface which is distinct from the melting transition for this surface. The predicted roughening transition temperature is in excellent agreement with experimental results.

On the other hand, the predicted transition temperature for melting of the clean (110) surface is significantly higher than the experimental value for both lead and gold. The predicted temperature of the order–disorder transition for the 1×2-restructured gold surface is also higher than that found experimentally.

With these results in mind, the question posed in the introduction, regarding when the EAM/MD method is expected to be reliable, may be returned to. Two of the examples where the predicted temperature is too high involve surface melting. It is important to emphasize that the surface melting of Pb(110) and Au(110) occurs sequentially, layer by layer. Since the long-range fluctuations at melting are limited to the first few layers near the surface, the onset temperature of surface melting is not expected to be significantly affected by the approximating of the bulk with fixed layers. (This may be compared with the expected behaviour of the (111) surface for these metals. On this surface, sequential surface melting does not occur, and fluctuations over a macroscopic number of layers are expected when the surface melts. Consequently, the use of fixed layers would not be an appropriate approximation for studying melting on the (111) surface.) Moreover the Au 1×2 order–disorder transition occurs approximately 100 K below the surface melting temperature, and is therefore unlikely to be significantly affected by the fixed-layer approximation.

However, when considering the nature of the physical change in the surface layer it may be noted that both the surface melting of Au(110) and Pb(110) and the Au 1×2 order–disorder transition are examples of phase transitions with the corresponding rapid changes in quantities such as the correlation length. In this case, approximations such as truncating the interaction range may be sufficiently critical to result in large quantitative shifts in the temperature despite the qualitative temperature dependence being correct. The discontinuities that occur at zero temperature at θ_c in the case of Pb on Au(110) are reminiscent of a first-order transition; however, the changes at θ_c in this system and the roughening transition on the clean Pb surface are primarily relaxation phenomena. Possibly, in these cases, the effect of the truncated interaction range remains small.

Acknowledgments

This work was supported, in part, by the Natural Science and Engineering Research Council of Canada. One of us (KDB) thanks A J Slavin for comments on the arguments presented in the summary.

References

[1] Zhang Y and Slavin A J 1992 *J. Vac. Sci. Technol.* **10** 2371
Ma P and Slavin A J 1993 *J. Vac. Sci. Technol.* **11** 2003
Jones T L and Venus D 1994 *Surf. Sci.* **302** 126
[2] Perdereau J, Biberian J-P and Rhead G E 1974 *J. Phys. F: Met. Phys.* **4** 798
Biberian J-P 1978 *Surf. Sci.* **74** 437
[3] Imeson D and De'Bell K 1995 *J. Phys.: Condens. Matter* **7** L487
[4] Mei J, Davenport J W and Fernando G W 1991 *Phys. Rev.* B **43** 4653
[5] Johnson R A 1988 *Phys. Rev.* B **37** 3924
Johnson R A 1989 *Phys. Rev.* B **39**
[6] Imeson D 1995 *MSc Thesis* Queen's University, Kingston

[7] *CRC Handbook of Chemistry and Physics* 1990 71st edn, ed D R Lide (Boca Raton, FL: Chemical Rubber Company Press) pp 12–107
[8] Yang H-N, Lu T-M and Wang G-C 1989 *Phys. Rev. Lett.* **63** 1621
Heyraud J C and Metois J J 1987 *J. Cryst. Growth* **82** 269
Frenken J M W, Toennies J P and Woll Ch 1990 *Phys. Rev. Lett.* **60** 1727
Frenken J M W, Marée P M J and van der Veen 1986 *Phys. Rev.* B **34** 7506
Breuer U, Knauff O and Bonzel H P 1990 *Phys. Rev.* B **41** 10 848
[9] Tibbits P, Karimi M, Ila D, Dalins I and Vidali G 1991 *J. Vac. Sci. Technol.* A **9** 1937
[10] Clark D E, Unertl W N and Kleban P H 1986 *Phys. Rev.* B **34** 4379
[11] Wolf D, Jagodzinski H and Moritz W 1978 *Surf. Sci.* **77** 265
Wolf D, Jagodzinski H and Moritz W 1978 *Surf. Sci.* **77** 283
Campuzano J C, Foster M S, Jennings G, Willis R F and Unertl W 1985 *Phys. Rev. Lett.* **54** 2684
Campuzano J C, Jennings G and Willis R F 1985 *Surf. Sci.* **162** 484
[12] Ercolessi F, Iarlori S, Tomagnini O, Tosatti E and Chen X J 1991 *Surf. Sci.* **251** 645
[13] Daw M S and Foiles S M 1987 *Phys. Rev. Lett.* **59** 2756
[14] Hoss A, Nold M, von Blackenhagen P and Meyer O 1992 *Phys. Rev.* B **45** 8714
[15] Karimi M, Yang Z, Tibbits P, Ila D, Dalins I and Vidali G 1990 *Atomic Scale Calculations of Structure in Materials (MRS Symposia Proceedings 193)* ed M S Daw and M A Schulter (Pittsburgh, PA: Materials Research Society) p 83